scientific reports

Check for updates

OPEN

Structural, optical and microwave dielectric properties of $Ba(Ti_{1-x}Sn_x)_4O_9$, $0 \le x \le 0.7$ ceramics

Asad Ali[1,2]✉, Sarir Uddin[3], Madan Lal[4]✉, Abid Zaman[1], Zafar Iqbal[1] & Khaled Althubeiti[5]✉

Sn-doped $BaTi_4O_9$ (BT4) dielectric ceramics were prepared by a mixed oxide route. Preliminary X-ray diffraction (XRD) structural study shows that the ceramic samples have orthorhombic symmetry with space group (Pnmm). Scanning electron microscopy (SEM) shows that the grain size of the samples decreases with an increase in Sn^{4+} content. The presence of the metal oxide efficient group was revealed by Fourier transform infrared (FTIR) spectroscopy. The photoluminescence spectra of the ceramic samples reported red color ~ 603, 604, 606.5 and 605 nm with excitation energy ~ 2.06, 2.05, 2.04 and 2.05 eV for Sn^{4+} content with x = 0.0, 0.3, 0.5, and 0.7, respectively. The microwave dielectric properties of these ceramic samples were investigated by an impedance analyzer. The excellent microwave dielectric properties i.e. high dielectric constant ($\varepsilon_r = 57.29$), high-quality factor ($Q_f = 11{,}852$), or low-dielectric loss (3.007) has been observed.

Dielectric ceramic materials are frequently used in modern telecommunication systems like satellite modules and cellular mobile phones. Layered-structured dielectric materials have been widely investigated for their potential use in ferroelectric random access memories (FeRAM) and piezoelectric devices. Ferroelectric and piezoelectric ceramic materials are broadly used in a range of applications such as sensors, actuators, transducers, pulse signal circuits, spacecraft, X-ray equipment, weapons, medical devices, and transportation. The dielectric component used in these devices is called dielectric resonators (DR). The optimum commercial dielectric properties of these ceramics included excellent dielectric constant (ε_r), good quality factor (Q_f) or low tangent loss (tan σ), and near to zero temperature coefficient at resonant frequency (τ_f)[1–6]. For example, a dielectrically loaded antenna requires; ε_r from 20 to 85, $(Q) \ge 10{,}000$, and τ_f close to zero[7,8]. Sometimes quality factor is expressed as the product of Q and f_o (resonant frequency) i.e. $(Q \times f_o)$. The dielectric constant (ε_r) and dielectric loss (tan σ) decrease with resonant frequency (f_o), which suggests that electric dipoles and interfaces play an important role at the lower frequency range. The decrease in dielectric constant with resonant frequency can be explained based on Koops theory, reported by Praveena and Varma[9]. A relatively good dielectric constant is required for the miniaturization of devices and low tangent loss is required for noise reduction with zero τ_f, which is important for the temperature stability of the DR[2]. From the manufacturing point of view, it is very difficult to obtain compounds with all three optimum properties along with a low cost. Among oxides compounds, $BaTi_4O_9$ (BT4) is one of the dielectric materials that may be used in the microwave domain as first reported by Rase and Roy[10]. It has been recorded that $BaTi_4O_9$ ceramics have $\varepsilon_r = 37.3$, $Q = 27{,}200$ GHz and $\tau_f = +15$ ppm/°C[11]. On the other side, wet chemical methods (i.e. sol–gel, co-precipitation, or hydrothermal) can be used for the preparation of titanates ceramics[12]. The optical, structural, microstructural, and microwave properties of $BaTi_4O_9$ ceramic samples with various dopant elements have been extensively studied at microwave frequency. Many researchers studied the effects of B site cation substitutions and dielectric properties of those samples affected by the substitution of larger ionic radius (Sn^{4+}) for smaller ionic radius (Ti^{4+}) ions[13–15]. In this way, Veenhuis et al. processed compounds with good dielectric properties which have been used in the field of advanced laser technology and optical storage devices[16].

In the present time, BT4 has been investigated broadly because of its good Q_f, high ε_r, and small τ_f. Because used widely in microwave dielectric resonator applications, patch antenna, microwave telecommunication

[1]Department of Physics, Riphah International University, Islamabad 44000, Pakistan. [2]Department of Physics, Government Post Graduate College, Nowshera, KP, Pakistan. [3]Department of Physics, Government Degree College Hayatabad, Peshawar 25000, Pakistan. [4]Department of Physics, Akal College of Basic Sciences, Eternal University, Sirmour, H.P 173101, India. [5]Department of Chemistry, College of Science, Taif University, Taif 21944, Saudi Arabia. ✉email: kasadiiui@gmail.com; madan.physics26@gmail.com; k.althubeiti@tu.edu.sa

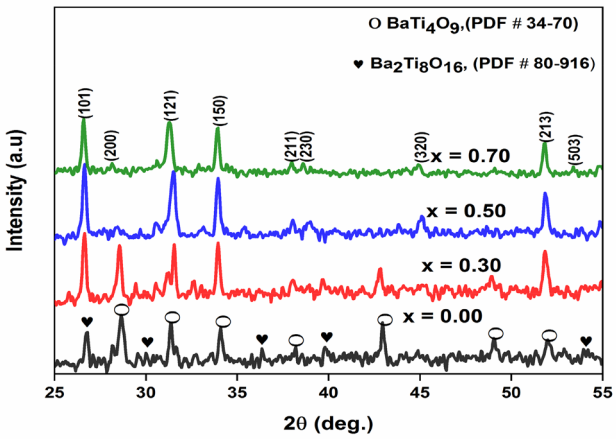

Figure 1. XRD pattern of $Ba(Ti_{1-x}Sn_x)_4O_9$, $0 \le x \le 0.7$ ceramics.

devices, etc. During the densification of these titanates at the very high sintering temperature, enhanced dielectric properties are observed due to the phase and compositional defects (fluctuations) (i.e. because of the partial reduction of Ti^{4+} to Ti^{3+} ion)[17]. The aim of the present work, to achieve a material with enhanced structural and dielectric properties for device application. In this report, we describe the synthesis (i.e.via the mixed oxide method) and the structural, optical, and microwave dielectric properties of Sn-doped $BaTi_4O_9$ ceramics. The calcined powders and sintered pellets obtained were characterized by XRD (X-ray diffraction), SEM (scanning electron microscopy), impedance analyzer, and FTIR (Fourier transform infra-red). The microwave dielectric properties of ceramic samples are discussed in terms of their physical and chemical characteristics.

Materials and methods

The starting raw materials along with purity grades were: $BaCO_3$ (Merck, Germany, 99.9%), TiO_2 (Aldrich Chemical Company, Inc., U.S.A, 99.9%), and SnO_2 (Strem, Chemicals, U.S.A, 99.9%) used to make the solid solutions of $Ba(Ti_{1-x}Sn_x)_4O_9$, $0 \le x \le 0.7$ by using mixed oxides route. These raw materials were weighted according to stoichiometric ratio and mixed for 12 h in distilled water by using horizontal ball milling. Then the slurry was dried in a microwave oven at 100 °C for one day and calcined at 1100 °C for 3 h in a nickel crucible in the air atmosphere with a heating–cooling rate of 10 °C/min. The calcined powders were grinded for 60 min with a mortar and pistol manually to avoid agglomerations. Then pressed 0.6–0.8 gm of powder in cylindrical pellets of thickness 2 mm and diameter 10 mm by using a hydraulic press (CARVER, USA) with a pressure of 80 MPa. Thereafter, these green pellets were sintered at 1320 °C temperature in the open air for 4 h with a heating–cooling rate of 10 °C/min. The XRD patterns of the compounds were recorded at room temperature using an X-ray powder diffractometer (JDX-3532, JEOL, Japan) with Cu Ka radiation (k = 1.5405 Å) in a wide range of Bragg angles ($20° \le 2\theta \le 60°$) at a scanning rate of 2 deg min^{-1}. The experimental density of the samples was measured by Archimedes' principle using a density meter (MD-3005, Germany). Scanning electron microscopy (SEM, JEOL 7600F) was used to study the microstructure of the dense pellets. The optical properties of these ceramics were done by using the Fourier transformation infrared spectroscopy (FTIR, Perkin-Elmer) and PL spectroscopy. Dielectric properties were measured at microwave frequencies by LCR meter (Agilent 4287 A).

Results and discussions

XRD analysis. Figure 1 represents the XRD patterns of $Ba(Ti_{1-x}Sn_x)_4O_9$, $0 \le x \le 0.7$ ceramics at room temperature. The main peaks corresponding to (200), (121), (150), (211), (230), (320), (213), (503) planes are well-matched with PDF card number 34–70 of $BaTi_4O_9$ ceramics and have an orthorhombic structure with space group (Pnmm). Some of the secondary phases of $Ba_2Ti_8O_{18}$ are detectable with PDF card number 0080–0916. It can be noted from Fig. 1 that the peaks shifted toward the lower 2θ values and representing the cell volume expansion with increasing the Sn^{4+} contents. This might be due to the inhomogeneity, micro-strain, or maybe due to the substitution of the relatively larger cation ions of Sn^{4+} (~ 0.69 Å) for the smaller cation of Ti^{4+} (~ 0.64 Å)[18]. The calculated lattice parameters (i.e. 'a', 'b', and 'c') increases with Sn^{4+} content. This increase in the lattice parameters may result in the phase transition from orthorhombic to a tetragonal structure. The average crystallite size of these samples was calculated by using Debye Scherer's formula[19]. The observed average crystallite size and lattice parameters are given in Table 1.

$$\text{Crystallite size, } D = \frac{0.9\lambda}{\beta \text{Cos}\theta} \tag{1}$$

where 'θ' is the brags angle, 'λ' is the wavelength of the incident radiation, and 'β' is the full-width of half-maximum (FWHM). The average crystallite size of these samples was lie in the range of 30–90 nm.

Composition (x)	Lattice parameters (Å)			Volume (Å^3)	Structure (space group)	Average crystallite size (D) nm
	a	B	c			
0.0	4.012	5.681	5.703	64.4	Orthorhombic (Pnmm)	90
0.3	4.024	4.024	4.045	65.1		50
0.5	4.036	4.036	4.057	65.7	Tetragonal (P4*mm*)	30
0.7	4.058	4.058	4.042	66.3		70

Table 1. Lattice parameters of $Ba(Ti_{1-x}Sn_x)_4O_9$, $0 \le x \le 0.7$ ceramics obtained from XRD.

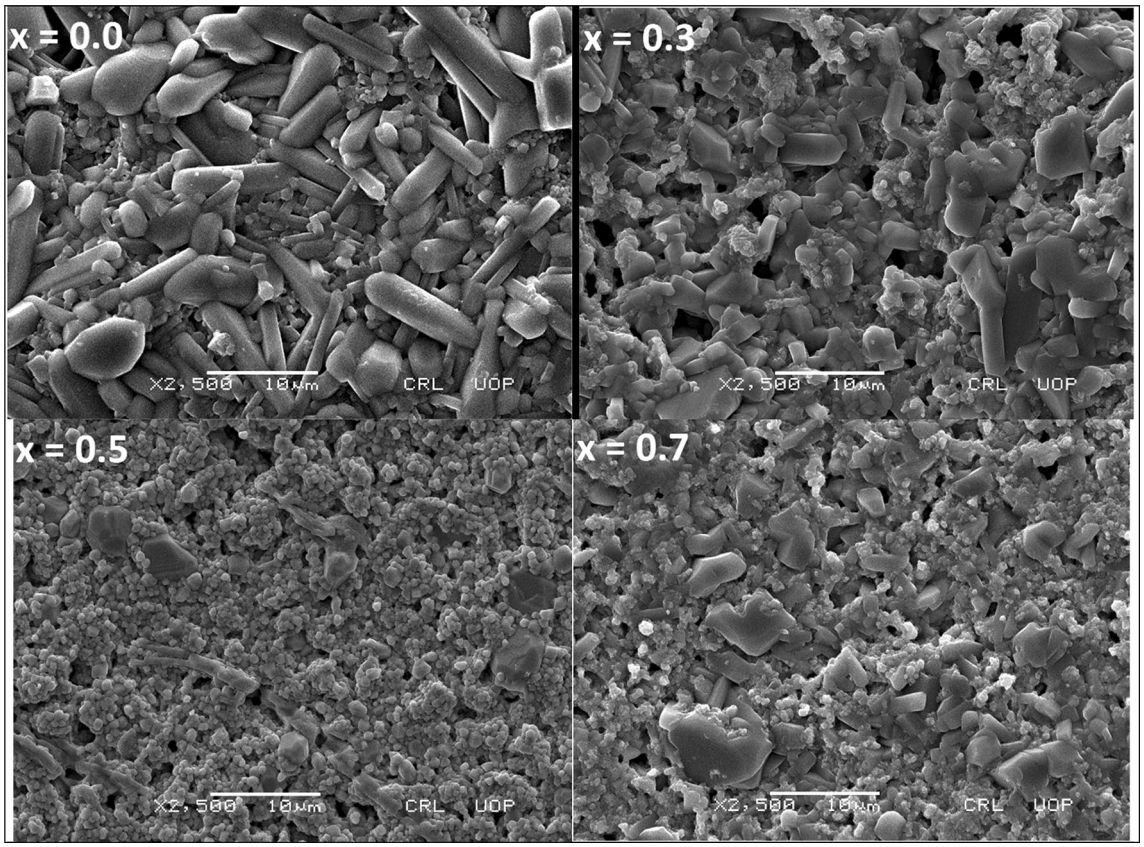

Figure 2. SEM Micrograph of $Ba(Ti_{1-x}Sn_x)_4O_9$, $0 \le x \le 0.7$ ceramics.

Composition (x)	ρ_{th} (gm/cm^3)	ρ_{ex} (gm/cm^3)	ρ_{re} (%)	ϵ_r	Porosity (%)	Average grain size (µm)
0.0	5.9	4.5	76.3	30.08	23.72	10.7
0.3	4.953	4.48	90.5	37.57	9.55	6.45
0.5	5.611	5.58	99.4	57.29	0.55	2.54
0.7	5.347	5.25	98.2	46.63	1.81	5.56

Table 2. Physical properties of $Ba(Ti_{1-x}Sn_x)_4O_9$, $0 \le x \le 0.7$ sintered ceramics.

Microstructure analysis. SEM images were used to calculate the average grain size and density of $Ba(Ti_{1-x}Sn_x)_4O_9$, $0 \le x \le 0.7$ ceramics (as shown in Fig. 2). It is clear from the figure that two types of surface morphologies are present in all samples (i.e. rod-like and spherical-like particles). The relative densities are increased, as the Sn^{4+} doping content increased in the base sample. The existence of cavities in the denser pellets confirms the existence of porosity. Thus, an increase in the relative density and decrease in the porosity was observed as the Sn content increased[20]. The porosity of these samples was calculated using Eq. (2) shown in Table 2.

$$\text{Porosity} = \left(\frac{\rho_{th} - \rho_{ex}}{\rho_{th}}\right) \times 100\% \quad (2)$$

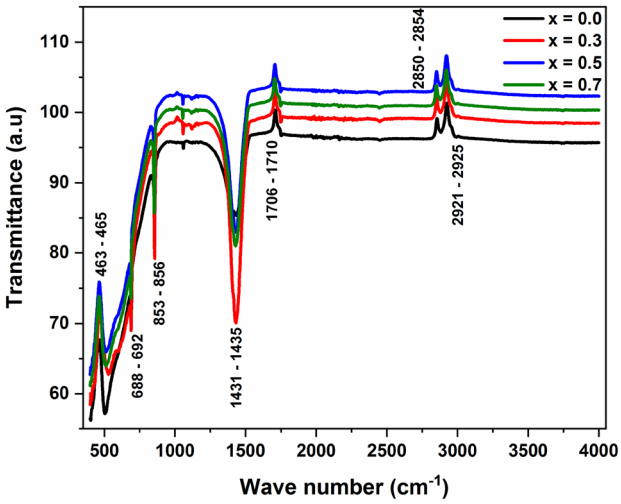

Figure 3. FTIR spectra of $Ba(Ti_{1-x}Sn_x)_4O_9$, $0 \le x \le 0.7$ ceramics.

where ρ_{th} = theoretical density and ρ_{ex} = experimental density (calculated using Archimedes' principle). The observed average grain size varies from ~ 10.7 to ~ 2 μm as dopant content x varies from 0.0 to 0.7. At x = 0.5, the Sn^{4+} doped $BaTi_4O_9$ system has a smaller average grain size of 0.8 μm with a more uniform grain size distribution. Thus, high densification (~ 99.4%) and low porosity (~ 0.55%) were achieved with Sn^{4+} = 0.5 content which reduces the growth of grains.

Optical properties. Figure 3 represents the FTIR spectra of $Ba(Ti_{1-x}Sn_x)_4O_9$, $0 \le x \le 0.7$ ceramics at room temperature. The peaks that appear near ~ 2852, ~ 2922, and ~ 1433 cm^{-1} represents the symmetric, asymmetric, and bending vibrations of the H-C-H group, respectively[21]. Peaks appearing at ~ 854 cm^{-1} show the vibrational mode which relates to the stretching mode of the O-Ti–O system in the ceramic samples that confirmed the presence of $BaTi_4O_9$ structures[22]. The absorption mode appearing at ~ 690 cm^{-1} represents the Ti–O stretching mode of the octahedral group in complex perovskite structure[23,24], as this mode appears only in $BaTi_4O_9$ ceramics. Furthermore, the structure of the $BaTi_4O_9$ ceramic sample has been confirmed by the XRD result.

Photoluminescence spectroscopy of $Ba(Ti_{1-x}Sn_x)_4O_9$, $0 \le x \le 0.7$ ceramics are shown in Fig. 4. The optical emission spectra are recognized as the recombination of electrons and holes in the state of transfer of carriers ions. By using Eq. (3), we have found the value of excitation energy of the samples.

$$E = hc/\lambda \tag{3}$$

where E = optical excitation energy, h = Plank's constant (~ 6.63×10^{-34} Js) c = velocity of light (3×10^8 m/s) and λ is the emission wavelength. Emission at photoluminescence peak of the samples were recorded at ~ 603, 604, 606.5 and 605 nm with excitation energy ~ 2.06, 2.05, 2.04 and 2.05 eV for x = 0.0, 0.3, 0.5, and 0.7 content of Sn^{4+} dopant, respectively. Photoluminescence is a multi-photonic process that is an optical energy emission occurred in the optical range by many vibrational modes within the samples[25]. Within the energy band-gap, the photoluminescence process confirmed that due to localizing state the order/disorder structure may be affected directly. Hence, the structural order/disorder may be increased with increasing the energy band gap[26]. It was recorded that a broad-emission spectrum was located at ~ 604 nm and have an optical excitation energy (~ 2.06 eV) which was smaller than the energy band gap of extremely ordered $BaTi_4O_9$ ceramics located at ~ 558 nm (~ 2.23 eV) which may be due to the absence of oxygen vacancy[27]. In the photoluminescence spectrum, the red color may occur due to the oxygen vacancy.

Microwave dielectric properties. The variation of the relative permittivity (ε_r) and tangent loss (tanδ) values of $Ba(Ti_{1-x}Sn_x)_4O_9$, $0 \le x \le 0.7$ sintered ceramics versus frequency at room temperature is shown in Fig. 5. Due to increasing frequency, the values of ε_r and tanδ decrease exponentially in the samples. The high value of ε_r at resonant frequency (f_o) can be described based on:

(1) According to Maxwell–Wagner's model, the dielectric materials are consist of fine conductive grains which are surrounded by grain boundaries. Large polarization is caused by the motion of charge carriers from grain to the grain surface.
(2) The ionic polarization
(3) The majority are due to crystal defects, vacancies, and grain defects etc[28,29].

The increase in ε_r values with Sn^{4+} contents may be recognized by the substitution of a larger ionic radius of Sn^{4+} (~ 0.69 Å) cation for a smaller ionic radius of Ti^{4+} (~ 0.64 Å) cation[30]. To increasing the bond length of complex perovskite (i.e. AB_4O_9) the larger ionic radius cation may be substituted at B-site cation. The Sn^{4+} contents

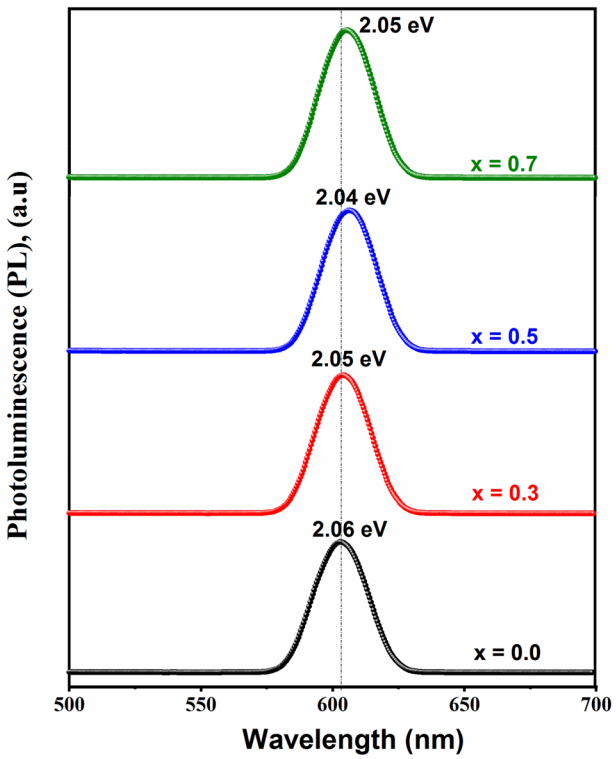

Figure 4. PL spectra of $Ba(Ti_{1-x}Sn_x)_4O_9$, $0 \le x \le 0.7$ ceramics.

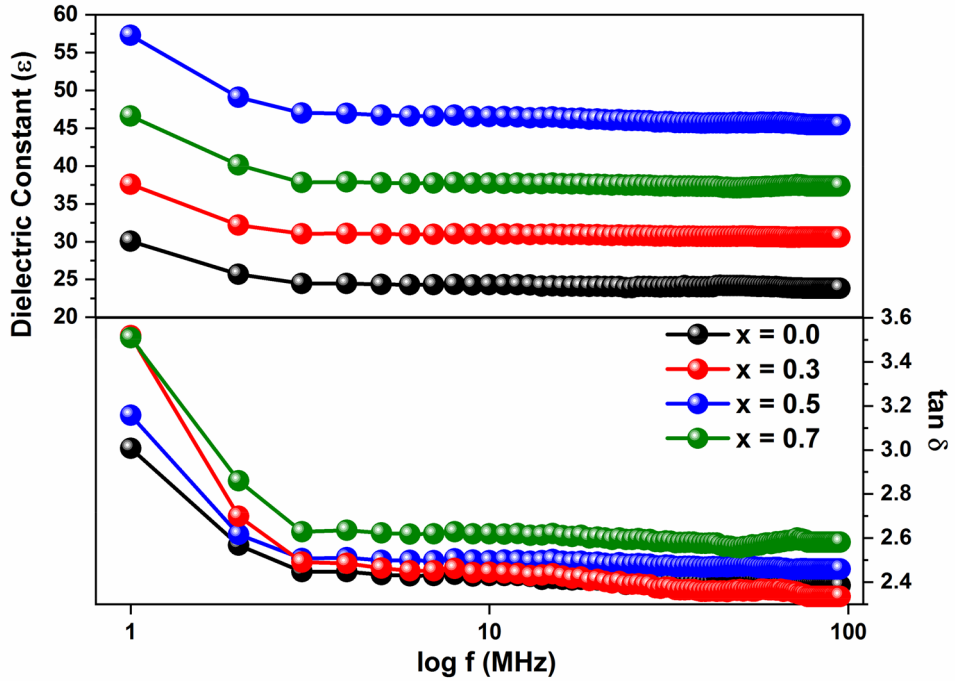

Figure 5. Frequency dependence of Dielectric constant (ε) and dielectric loss (tanδ) of $Ba(Ti_{1-x}Sn_x)_4O_9$, $0 \le x \le 0.7$ ceramics.

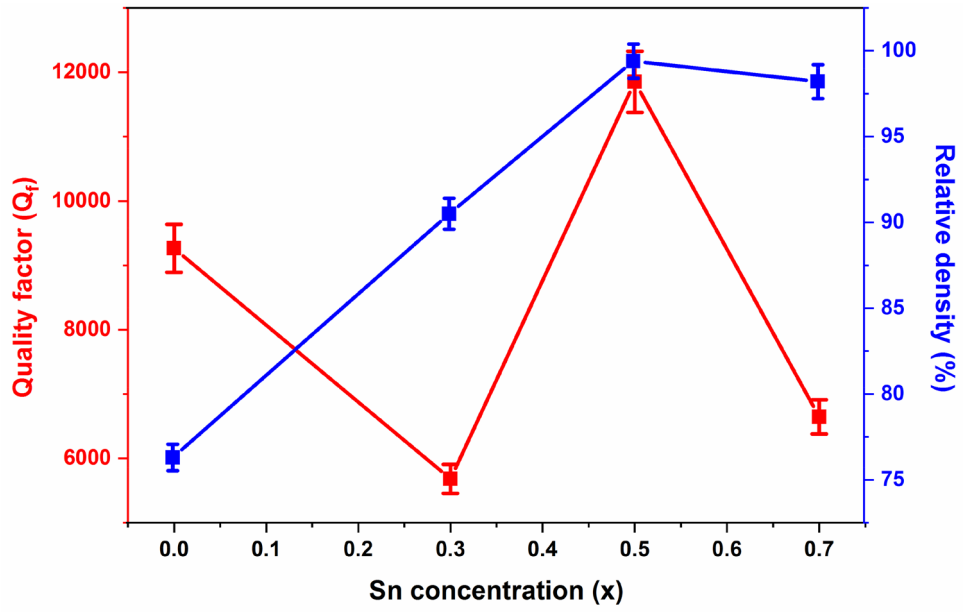

Figure 6. Variation of relative density and Quality factor (Q_f) versus Sn^{4+} contents of $Ba(Ti_{1-x}Sn_x)_4O_9$, $0 \le x \le 0.7$ ceramics.

greatly affected the microwave dielectric properties due to high ionic polarization[31,32]. The maximum dielectric constant is obtained at $x = 0.5$ at maximum relative density (i.e. at low porosity). Because charge carriers need a medium to propagate and hence dielectric constant decreases with increasing material porosity[33,34]. Dielectric loss decreases with frequency due to the space charge polarization in all samples. At the lowest frequency, the maximum tangent loss occurs due to the presence of defects, impurities, and porosity in the ceramic samples[35].

In general, the microwave dielectric properties of ceramics are dependent on intrinsic and extrinsic factors. The intrinsic properties are due to the interaction of materials phonons with the applied ac field. Thus the intrinsic properties also depend upon the crystal symmetry as observed in many single crystals[36]**.** The extrinsic properties are due to the imperfection in the crystal structure such as dopants or impurity atoms, grain boundaries, vacancies, order–disorder, secondary phases, etc[36–40]. Mostly, extrinsic factors are process-dependent and can be optimized. In this report, the sintering of these ceramic samples was done at a very high temperature (i.e. > 1300 °C for 4 h). The sintering at a high temperature may be causing the partial reduction of Ti^{4+} to Ti^{3+} ions. When Sn^{4+} is doped, it helps to maintain Ti^{4+} due to the following reaction:

$$Sn^{4+} + Ti^{3+} \rightleftharpoons Sn^{3+} + Ti^{4+}$$

and, thus control the reduction of Ti^{4+} to Ti^{3+} ions.

Therefore, at high-temperature sintering, a sintered layer acts as a shield that prevents the transport of oxygen to the core. Due to the lack of oxygen at the core, oxygen vacancies or titanium interstitials are produced. The presence of vacancies in the lattice is responsible for damping of phonon modes and hence maybe leads to enhancement of dielectric properties and Q-factors[36,41,42].

The variation of quality factor (Q_f) and relative density (%) of $Ba(Ti_{1-x}Sn_x)_4O_9$ sintered ceramics as a function of composition (x) is shown in Fig. 6. Initially, the quality factor decreases from 9264.49 to 5681.16 with increasing Sn^{4+} content (from 0 to 0.3). The observed decrease in the value of Q_f may be accepted due to the substitution of larger Sn^{4+} cation ion on the B-site cation, contributing to harmonic vibrational modes[43–45] and another reason may be the phase transition. Additionally, an increase in Sn^{4+} content leads to a high Q_f value, which may occur due to: (1) The phonon modes of B-site harmonic, and (2) Relative density of the ceramic samples.

The variation of ac conductivity of $Ba(Ti_{1-x}Sn_x)_4O_9$, $0 \le x \le 0.7$ sintered ceramics versus frequency is shown in Fig. 7. It is clear from the graph that ac conductivity depends upon the frequency and does not show any significant variation at the lowest frequency. The maximum value of ac conductivity at a lower frequency may be due to the rising state of localization in the hopping process. By the application of electric field, the hopping frequency of the charge carrier increased which result in the highest value of ac conductivity towards the high-frequency region[46].

Conclusion

Solid solutions of $Ba(Ti_{1-x}Sn_x)_4O_9$, $(0 \le x \le 0.7)$ ceramics were fabricated through a mixed-oxide route. The average crystallite size of these ceramic samples lies in the range of 30–90 nm with phase change from orthorhombic (space group = Pnmm) to Tetragonal (P4*mm*) structure. Sintered ceramics attained 99.5% of the theoretical density at content ($x = 0.5$) and fine grain growth with uniformity was achieved. Photoluminescence confirmed that the present state of localization within the band-gap may affect the structural order/disorder. The dielectric

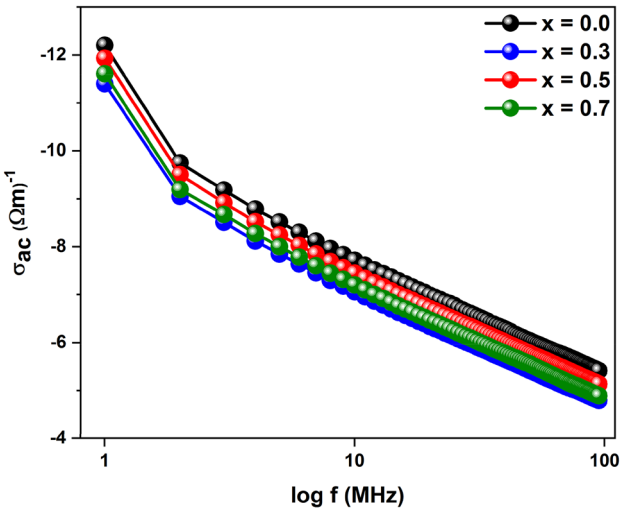

Figure 7. Variation of ac conductivity as a function of the frequency of $Ba(Ti_{1-x}Sn_x)_4O_9$, $0 \le x \le 0.7$ ceramics.

properties of sintered ceramic samples showed $\varepsilon_r = 57.29$, and high $Q_f = 11{,}852$. The increase in ac conductivity is due to the hopping mechanism. Based on the above-obtained results, these ceramic materials can be used for filter applications.

Data availability

The data of this study are available from the corresponding author upon reasonable request.

Received: 27 May 2021; Accepted: 27 August 2021
Published online: 09 September 2021

References

1. Richtmyer, R. Dielectric resonators. *J. Appl. Phys.* **10**, 391–398 (1939).
2. Sebastian, M. T. *Dielectric Materials for Wireless Communication* (Elsevier, New York, 2010).
3. Vijay Kumar, H. & Muralidhar Nayak, M. A highly efficient iron doped $BaTiO_3$ nanocatalyst for the catalytic reduction of nitrobenzene to azoxybenzene. *RSC Adv.* **4**, 18881–18884 (2014).
4. Kumar, S. & Varma, K. Dielectric relaxation in bismuth layer-structured $BaBi_4Ti_4O_{15}$ ferroelectric ceramics. *Curr. Appl. Phys.* **11**, 203–210 (2011).
5. Patel, S. *et al.* Tuning of dielectric, pyroelectric and ferroelectric properties of 0.715 $Bi_{0.5}Na_{0.5}TiO_3$–0065 $BaTiO_3$–022 $SrTiO_3$ ceramic by internal clamping. *AIP Adv.* **5**, 087145 (2015).
6. Sebastian, M., Ubic, R. & Jantunen, H. Low-loss dielectric ceramic materials and their properties. *Int. Mater. Rev.* **60**, 392–412 (2015).
7. Mirsaneh, M., Leisten, O. P., Zalinska, B. & Reaney, I. M. Circularly polarized dielectric-loaded antennas: Current technology and future challenges. *Adv. Func. Mater.* **18**, 2293–2300 (2008).
8. Muhammad, R., Iqbal, Y. & Reaney, I. M. New low loss A9B9O31 (A= La; B= Ti, Mg, Sc, Fe, Al, Ga) ceramics for microwave applications. *J. Alloys Compd.* **646**, 368–371 (2015).
9. Praveena, K. & Varma, K. Ferroelectric and optical properties of $Ba_5Li_2Ti_2Nb_8O_{30}$ ceramics potential for memory applications. *J. Mater. Sci. Mater. Electron.* **25**, 3103–3108 (2014).
10. Rase, D. & Roy, R. Phase equilibria in the system BaO–TiO_2. *J. Am. Ceram. Soc.* **38**, 102–113 (1955).
11. O'Bryan, H. Jr., Thomson, J. Jr. & Plourde, J. A new BaO–TiO_2 compound with temperature-stable high permittivity and low microwave loss. *J. Am. Ceram. Soc.* **57**, 450–453 (1974).
12. Cernea, M. Microwave dielectric properties of $BaT_{14}O_9$–Nd_2O_3, $BaT_{14}O_9$–Sm_2O_3 and $BaT_{14}O_9$–WO_3 ceramics. *J. Optoelectron. Adv. Mater.* **9**, 3790–3794 (2007).
13. Mueller, V., Beige, H. & Abicht, H.-P. Non-Debye dielectric dispersion of barium titanate stannate in the relaxor and diffuse phase-transition state. *Appl. Phys. Lett.* **84**, 1341–1343 (2004).
14. Lu, S., Xu, Z. & Chen, H. Tunability and relaxor properties of ferroelectric barium stannate titanate ceramics. *Appl. Phys. Lett.* **85**, 5319–5321 (2004).
15. Shvartsman, V., Kleemann, W., Dec, J., Xu, Z. & Lu, S. Diffuse phase transition in Ba $Ti_{1-x}SnxO_3$ ceramics: An intermediate state between ferroelectric and relaxor behavior. *J. Appl. Phys.* **99**, 124111 (2006).
16. Veenhuis, H. *et al.* Light-induced charge-transport properties of photorefractive barium-calcium-titanate crystals doped with rhodium. *Appl. Phys. B* **70**, 797–801 (2000).
17. Ma, H. *et al.* $BaTi_4O_9$ mesocrystal: Topochemical synthesis, fabrication of ceramics, and relaxor ferroelectric behavior. *J. Alloys Compd.* **777**, 335–343 (2019).
18. Ali, A. *et al.* Dielectric and optical properties of tin-doped barium tetra titanate ceramics. *Rev. Rom. Mater.* **50**, 448–452 (2020).
19. Lal, M. *et al.* Study of structural and magnetoelectric properties of 1–x ($Ba_{096}Ca_{004}TiO_3$)–x ($ZnFe_2O_4$) ceramic composites. *J. Mater. Sci. Mater. Electron.* **29**, 80–85 (2018).
20. Kumar, M. M., Srinivas, K. & Suryanarayana, S. Relaxor behavior in $BaTiO_3$. *Appl. Phys. Lett.* **76**, 1330–1332 (2000).
21. Gupta, S. & Subramanian, V. Encapsulating $Bi_2Ti_2O_7$ (BTO) with reduced graphene oxide (RGO): An effective strategy to enhance photocatalytic and photoelectrocatalytic activity of BTO. *ACS Appl. Mater. Interfaces.* **6**, 18597–18608 (2014).
22. Sun, D. *et al.* Investigation on FTIR spectrum of barium titanate ceramics doped with alkali ions. *Ferroelectrics* **355**, 145–148 (2007).

23. Pavlović, N. & Srdić, V. V. Synthesis and structural characterization of Ce-doped bismuth titanate. *Mater. Res. Bull.* **44**, 860–864 (2009).
24. Yadav, K. Optical and dielectric properties of $Bi_2Ti_2O_7/Bi_4Ti_3O_{12}$ nanocomposite. *Mater. Today Proc.* **28**, 153–157 (2020).
25. Longo, V. *et al.* Structural conditions that leads to photoluminescence emission in $SrTiO_3$: An experimental and theoretical approach. *J. Appl. Phys.* **104**, 023515 (2008).
26. Leite, E. R. *et al.* The origin of photoluminescence in amorphous lead titanate. *J. Mater. Sci.* **38**, 1175–1178 (2003).
27. El Marssi, M., Le Marrec, F., Lukyanchuk, I. & Karkut, M. Ferroelectric transition in an epitaxial barium titanate thin film: Raman spectroscopy and x-ray diffraction study. *J. Appl. Phys.* **94**, 3307–3312 (2003).
28. Kaur, M. *et al.* Effect on the dielectric properties due to In–N co-doping in ZnO particles. *J. Mater. Sci. Mater. Electron.* **32**, 8991–9004 (2021).
29. Liu, B., Hu, C. C., Huang, Y. H., Bafrooei, H. B. & Song, K. X. Crystal structure, infrared reflectivity spectra and microwave dielectric properties of $CaAl_2O_4$ ceramics with low permittivity. *J. Alloys Compd.* **791**, 1033–1037 (2019).
30. Shannon, R. D. Revised effective ionic radii and systematic studies of interatomic distances in halides and chalcogenides. *Acta Crystallogr. Sect. A Cryst. Phys. Diffract. Theor General Crystallogr.* **32**, 751–767 (1976).
31. Muhammad, R., Iqbal, Y. & Reaney, I. M. Structure and microwave dielectric properties of $La_{5-x}SrxTi_{4+x}Ga_{1-x}O_{17}$ ceramics. *J. Mater. Sci.* **50**, 3510–3516 (2015).
32. Iqbal, Y. & Muhammad, R. Microwave dielectric properties of Mg-doped $SrLa_4Ti_5O_{17}$ layered perovskite. *J. Mater. Sci. Mater. Electron.* **27**, 1314–1317 (2016).
33. Weng, M.-H., Liang, T.-J. & Huang, C.-L. Lowering of sintering temperature and microwave dielectric properties of $BaTi_4O_9$ ceramics prepared by the polymeric precursor method. *J. Eur. Ceram. Soc.* **22**, 1693–1698 (2002).
34. Liu, B. *et al.* Enhancement of densification and microwave dielectric properties in LiF ceramics via a cold sintering and post-annealing process. *J. Eur. Ceram. Soc.* **41**, 1726–1729 (2021).
35. Das, S., Das, S. & Sutradhar, S. Effect of Gd3+ and Al3+ on optical and dielectric properties of ZnO nanoparticle prepared by two-step hydrothermal method. *Ceram. Int.* **43**, 6932–6941 (2017).
36. Freer, R. & Azough, F. Microstructural engineering of microwave dielectric ceramics. *J. Eur. Ceram. Soc.* **28**, 1433–1441 (2008).
37. Reaney, I. M. & Iddles, D. Microwave dielectric ceramics for resonators and filters in mobile phone networks. *J. Am. Ceram. Soc.* **89**, 2063–2072 (2006).
38. Muhammad, R., Iqbal, Y., Rambo, C. R. & Khan, H. Research trends in microwave dielectrics and factors affecting their properties: A review. *Int. J. Mater. Res.* **105**, 431–439 (2014).
39. Kumar, S., Raju, V. & Kutty, T. Preparation of $BaTi_4O_9$ and $Ba_2Ti_9O_20$ ceramics by the wet chemical gel-carbonate method and their dielectric properties. *Mater. Sci. Eng., B* **142**, 78–85 (2007).
40. Liu, L., Flores, M. & Newman, N. Microwave loss in the high-performance dielectric Ba $(Zn_{1/3}Ta_{2/3})$ O_3 at 4.2 K. *Phys. Rev. Lett.* **109**, 257601 (2012).
41. Cheng, C.-M., Yang, C.-F., Lo, S.-H. & Tseng, T.-Y. Sintering $BaTi_4O_9/Ba_2Ti_9O_{20}$-based ceramics by glass addition. *J. Eur. Ceram. Soc.* **20**, 1061–1067 (2000).
42. Liu, B. *et al.* Novel low-εr MGa_2O_4 (M= Ca, Sr) microwave dielectric ceramics for 5 G antenna applications at the Sub-6 GHz band. *J. Eur. Ceram. Soc.* **41**, 5170–5175 (2021).
43. Zhou, D., Randall, C. A., Wang, H., Pang, L. X. & Yao, X. Microwave dielectric properties trends in a solid solution $(Bi_{1-x}Lnx)$ $2Mo_2O_9$ (Ln= La, Nd, $0.0 \le x \le 0.2$) system. *J. Am. Ceram. Soc.* **92**, 2931–2936 (2009).
44. Liu, B. *et al.* High quality factor cold sintered LiF ceramics for microstrip patch antenna applications. *J. Eur. Ceram. Soc.* **41**, 4835–4840 (2021).
45. Jin, D. H. *et al.* Boosting densification and microwave dielectric properties in cold sintered BaF2 ceramics for 5.8 GHz WLAN applications. *J. Alloys Compd.* **886**, 161141 (2021).
46. Khan, R. *et al.* Influence of oxygen vacancies on the structural, dielectric, and magnetic properties of (Mn, Co) co-doped ZnO nanostructures. *J. Mater. Sci. Mater. Electron.* **29**, 9785–9795 (2018).

Acknowledgements

Author Khaled Althubeiti is thankful to Researcher Supporting Project (TURSP-2020/241) at Taif University for the financial support.

Author contributions

A.A. and A.Z. prepared samples and write the manuscript. S.U. helps in measurements. Z.I. supervises this research. M.L. and K.A. did the final writing-review, corrections, and editing. All the authors read and approve the final manuscript.

Competing interests

The authors declare no competing interests.

Additional information

Correspondence and requests for materials should be addressed to A.A., M.L. or K.A.

Reprints and permissions information is available at www.nature.com/reprints.

Publisher's note Springer Nature remains neutral with regard to jurisdictional claims in published maps and institutional affiliations.